Solar EUV Irradiance Uncertainties for Planetary Studies

Edward Michael Benjamin Thiemann[1], Francis G. Eparvier[1], Victoria Knoer[2], Abdulla Al Muharrami[3], and Robert James Lillis[4]

[1]Laboratory for Atmospheric and Space Physics
[2]University of Colorado
[3]Mohammed Bin Rashid Space Center
[4]University of California, Berkeley

November 26, 2022

Abstract

The MAVEN/EUVM solar soft x-ray (SXR) and Lyman-α measurements are compared with analogous measurements made from Earth to characterize the typical error introduced when phase-shifting solar EUV irradiance measurements made from Earth to other points in the solar system according to the 27.27 day synodic solar rotation period. The phase-shifting error, ε, measured at SXR and Lyman-α are extrapolated to the full EUV spectrum by assuming it is proportional to the variability that occurs over the 27-day timescale of solar rotation. Values for ε as a function of wavelength are reported and used to find the typical error for estimates of photoionization frequencies of some major species found in planetary upper atmospheres derived by phase-shifted EUV irradiance. This study finds that the typical extrapolation error for the CO photoionization frequency is 5.7% of the solar cycle mean value, and 87% of the typical 27-day variability.

Solar EUV Irradiance Uncertainties for Planetary Studies

E. M. B. Thiemann[1], F. G. Eparvier[1], V. Knoer[1], Abdulla Al Muharrami[2], and R. J. Lillis[3]

[1]Laboratory for Atmospheric and Space Physics, University of Colorado Boulder, USA.
[2]Mohammed Bin Rashid Space Center, Dubai, UAE. [3]Space Sciences Laboratory, University of Califorina Berkeley, USA.

Corresponding author: Edward Thiemann (thiemann@lasp.colorado.edu)

3665 Discover Drive, Boulder, CO 80303

Key Points:

- Calibrated irradiances measured from Mars are used to quantify phase-shift error at the 0-7 nm and Lyman-α bands.
- Phase-shift error is extrapolated to the ionizing EUV spectrum assuming proportionality to the 27-day variability.
- The phase-shift error for the ionizing irradiance and ionization frequencies of major species is comparable to the 27-day variability.

Abstract

The MAVEN/EUVM solar soft x-ray (SXR) and Lyman-α measurements are compared with analogous measurements made from Earth to characterize the typical error introduced when phase-shifting solar EUV irradiance measurements made from Earth to other points in the solar system according to the 27.27 day synodic solar rotation period. The phase-shifting error, ε_{ps}, measured at SXR and Lyman-α are extrapolated to the full EUV spectrum by assuming it is proportional to the variability that occurs over the 27-day timescale of solar rotation. Values for ε_{ps} as a function of wavelength are reported and used to find the typical error for estimates of photoionization frequencies of some major species found in planetary upper atmospheres derived by phase-shifted EUV irradiance. This study finds that the typical extrapolation error for the CO_2 photoionization frequency is 5.7% of the solar cycle mean value, and 87% of the typical 27-day variability.

Plain Language Summary

Solar Extreme Ultraviolet (EUV) radiation is the major source of energy to the upper atmospheres of the planets, and varies with time and location on the Sun's surface. This study uses direct measurements of EUV radiation made by the Mars Atmosphere and Volatile Evolution (MAVEN) probe at Mars to measure the accuracy of approximation techniques for estimating solar EUV radiation at other planets. This study finds that estimates of EUV radiation induced change in planetary atmospheres over periods of around 30 days can be off by nearly a factor of 2, with accuracy improving to about 6% when decade-long periods are considered.

1 Introduction

Solar extreme ultraviolet (EUV, 10-121 nm) radiation is the primary energy input to the upper and tenuous atmospheres of most planetary bodies. As such, accurate estimates of solar EUV irradiance are needed throughout the solar system in order to understand the dynamical, chemical and plasma processes occurring in these regions. Most robotic missions sent to explore upper and tenuous planetary atmospheres are not instrumented to measure solar irradiance in-situ, and instead rely on irradiance measurements made at Earth, which are extrapolated to the location of interest. The same methods are also needed to analyze telescope observations that depend on solar irradiance forcing. Extrapolations of solar ultraviolet (UV) and EUV irradiance are widespread in planetary science, having been used in studies of every planet in the solar system, as well as the dwarf planet Pluto and comets [e.g. Killen et al., 2001; Peter et al., 2014; Ramstad et al., 2015; Tsuchiya et al., 2011; Moore et al., 2009; Moore et al., 2011; Parkinson et al., 1990; Trafton and Stern, 1996; Johansson et al., 2017].

Solar irradiance is typically extrapolated by assuming that, over short time scales, solar EUV radiation emitted from a particular heliographic longitude (longitude of a feature on the Sun's surface) is constant, and the emissions into interplanetary space simply vary according to the sidereal rotation rate of 25.38 days (not to be confused with the 27.27 synodic rotation rate apparent from Earth), akin to the rotating beam from a lighthouse cyclically illuminating the surrounding darkness. Under the assumption of slowly varying EUV emission, EUV irradiance at a particular time and location in the solar system, say Θ(t), with a corresponding heliographic longitude can be estimated by averaging measurements of the solar irradiance when that same heliographic longitude is directed at Earth before and after it passes Θ(t). For example, suppose today the Earth-Mars-Sun angle was 90^{o}, with Mars oriented above the Sun's West limb as viewed from Earth. The EUV irradiance at Mars could be approximated by averaging measurements made from Earth 6.8 days ago with those made from Earth 20.45 days in the future, with the average weighted to bias the measurements occurring more closely in time, resulting in the earlier (later) measurement being weighted by 0.75 (0.25). The phase-shifted irradiance would then be scaled from Earth's distance from the Sun to that of Mars. The method for applying this phase-shifting and scaling is described in detail in Thiemann et al., [2017].

In reality, solar EUV radiation does indeed vary over the time-scale of solar rotation. The hot plasma where these emissions form is constantly evolving, and often fast. The most rapid changes occur during solar flares, during which for large flares, the solar EUV irradiance can temporarily double for tens of minutes [e.g. Woods et al., 2004; Chamberlin et al., 2018; Thiemann et al., 2018a]. At daily time-scales, the magnetic flux that is the fundamental source of energy to the EUV emitting plasma emerges and decays due to processes occurring at the Sun's surface and below, which are difficult (in the case of decay) if not impossible (in the case of emergence) to accurately predict [Arge et al., 2010]. These changes in the magnetic structure of the solar atmosphere drive corresponding changes in the solar EUV irradiance, ultimately causing the variability of the 11-year solar cycle.

In addition to being subject to spatiotemporal variability, solar EUV irradiance varies spectrally with time. The lines and continua that constitute the solar EUV spectrum form throughout the Sun's atmosphere, spanning regions with distinct variability. Emissions forming in the cooler chromosphere tend to be less variable than those forming in the hotter corona, with variability in the intermediate transition region falling somewhere in between, resulting in changes in both the magnitude and shape of the solar spectrum with time [e.g. Woods et al., 2018]. Further, the opacity of a particular emission will influence its variability [Chamberlin et al., 2007; Thiemann et al., 2018b], with optically thick emissions tending to be less variable.

At Earth, the most complete record of solar EUV spectral irradiance has been measured by the Solar EUV Experiment (SEE; Woods et al., 2005) instrument onboard the Thermosphere Ionosphere Mesosphere Energetics and Dynamics (TIMED) satellite and the EUV Variability Experiment (EVE; Woods et al., 2010) instrument onboard the Solar Dynamics Observatory. SEE has operated since 2002, but has uncorrected degradation beginning in 2012; and EVE has operated since 2010, but lost its 6 - 35 nm channel due to an electrical component failure. The other major solar EUV irradiance dataset was collected by the EUV Spectrometers onboard the Atmospheric Explorer E mission, which operated in the late 1970s. To account for both spectral and temporal gaps in the observational record, solar spectral irradiance models are used, which are driven by solar indices that capture the dominant sources of variability. These models tend to have random uncertainties <5 % and the same systematic absolute calibration uncertainties as the instruments used to calibrate them. This systematic uncertainty is typically 5-15%, and can be treated as a constant unknown bias. For a recent review of solar EUV irradiance variability models, see Section 1 of Thiemann et al., [2019].

There have been few instances of calibrated solar EUV irradiance being measured in-situ at other planets. Brace et al. [1988] derived solar EUV irradiance measurements at Venus using the Langmuir probes onboard the Pioneer Venus Orbiter (PVO), which were sensitive to photoelectron emission in the ~55-122 nm range. The photoelectron emission induced photocurrent serves as an index of solar EUV irradiance at Venus during the PVO mission and is comparable to the contemporaneous Earth-measured 10.7 cm solar radio flux (F10.7) and the solar 121.6 H I line irradiance (Lyman-α). The Mars Atmosphere and Volatile EvolutioN (MAVEN; Jakosky et al., 2015) orbiter, which has been at Mars from late 2014 through the present and is tasked with characterizing variability in the Mars upper atmosphere, includes the Extreme Ultraviolet Monitor (EUVM; Eparvier et al., 2015) to measure the solar EUV irradiance in-situ at

Mars. MAVEN/EUVM measures calibrated EUV irradiance in three wavelength bands, soft X-ray (hereafter, SXR), 17-22 nm and Lyman-α, which are representative of emissions forming in the hot corona, cooler corona and lower transition region, respectively. These measurements are used as inputs into the MAVEN/EUVM Level 3 spectral irradiance model data product, which estimates solar spectral irradiance at 1 nm sampling from 0.5 – 189.5 nm [Thiemann et al., 2017]. The direct, calibrated measurements made from Mars provide an opportunity to quantify the error introduced when phase-shifting EUV measurements made from Earth to other locations in the solar system.

This paper reports the uncertainty associated with phase-shifting EUV irradiance from Earth to other locations in the solar system by using two of the MAVEN/EUVM bands that have corresponding measurements made from Earth to quantify the phase-shifting error for moderately variable transition region emissions and highly variable hot corona emissions. These results are extrapolated to the full EUV solar spectrum, using measurements of variability as a function of wavelength made by TIMED/SEE and SDO/EVE. The phase-shifting error as a function of wavelength is then used to compute the error in extrapolating EUV irradiance and photoionization frequencies from Earth to other planets. This error is put in the context of different scales of solar variability and direct EUV irradiance measurements.

2 Data and Methods

The MAVEN/EUVM SXR and Lyman-α bands are cross-calibrated with analogous measurements from Earth. The SXR band is cross-calibrated with a near-identical channel of the EUV SpectroPhotometer (ESP; Didkovsky et al., 2009) instrument onboard SDO, which uses the same detector and filter technologies with minor differences in component thicknesses. Spectral irradiances in the SXR range are computed by driving the Synthetic Reference Spectra Model (hereafter, SynRef; Woods et al., 2008; Thiemann 2016) with the SXR derived photocurrents, which are scaled to the MAVEN/EUVM photocurrent calibration. The reason for working with the measured photocurrents rather than the higher level irradiances is ensure the same spectral assumptions are used when deriving irradiances from both measurements. The photocurrents are first cross-calibrated by (1) phase-shifting the SDO/ESP measurements to Mars' solar longitude (L_s), (2) smoothing the two datasets over 55-days (to remove variability occurring at the 27-day solar rotation time-scale) and (3) using a first-order linear least-squares fit to find the regression coefficients relating the photocurrent measurements. The cross-calibration fit of the two instruments' photocurrents is shown in Figure 1a. The end-result is a cross-calibration of the MAVEN/EUVM and SDO/ESP 0-7 nm sensors with the calibration uncertainty, σ_{cal}, ranging from 2% - 10% (the percent uncertainty is inversely proportional to irradiance) for the time period analyzed (late-2014 through mid-2017), respectively. Sample results, with ESP phase-shifted to Mars L_s and both measurements scaled to 1 AU are shown in Figure 1b.

MAVEN/EUVM measures solar Lyman-α irradiance using a broad-band (Full Width at Half Maximum (FWHM) of ~7nm) interference filter centered near 121 nm. 90% of the solar irradiance measured in this passband originates from the solar Lyman-α line. MAVEN/EUVM Lyman-α measurements are cross-calibrated with the SOLar STellar Irradiance Comparison Experiment (SOLSTICE; McClintock et al., 2005) onboard the SOlar Radiation and Climate Experiment (SORCE), which made contemporaneous measurements of solar Lyman-α irradiance at 0.1 nm spectral resolution. To ensure consistency between the two measurements, the MAVEN/EUVM solar Lyman-α measurements are cross-calibrated with measurements made from Earth with SORCE/SOLSTICE by first convolving the 0.1 nm resolution

SORCE/SOLSTICE spectral irradiance measurements with the MAVEN/EUVM Lyman-α filter transmission function. The SORCE/SOLSTICE values are then phase-shifted to Mars' L_s, where the same smoothing and fitting process applied to the SXR datasets is applied to cross-calibrate the two Lyman-α datasets. The fit between the convolved SORCE/SOLSTICE and MAVEN/EUVM data is shown in Figure 1c and the resulting σ_{cal} ranges from 0.42% to 0.5% for the time period analyzed. Ranges of σ_{cal} are given in Figures 1a and 1c. Figure 1d shows the phase-shifted SORCE/SOLSTICE data with the MAVEN/EUVM data, both scaled to 1 AU.

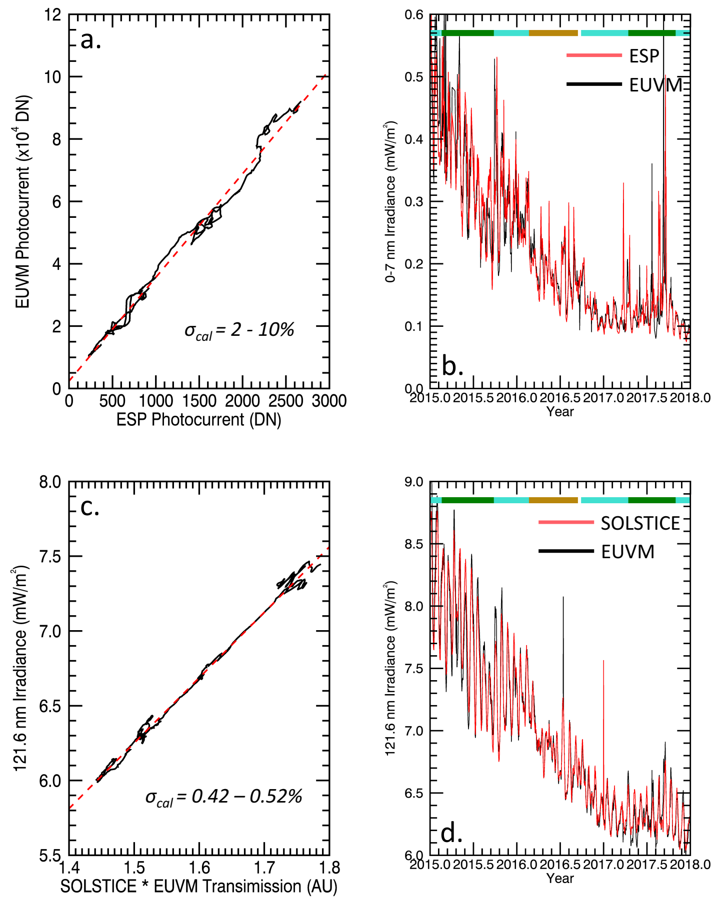

Figure 1. (a) Cross-calibration fits of the EUVM and ESP SXR derived photocurrents. (b) Comparison of SXR irradiance from EUVM and ESP phase-shifted to Mars L_s. (c) Cross-calibration fits of the EUVM Lyman-α band and the SOLSTICE spectra convolved with the EUVM filter transmission function. (d) Comparison of Lyman-α irradiance from EUVM and ESP phase-shifted to Mars. Differences between the curves in panels b and d are indicative of phase-shifting error. The color bar at the top of panels (b) and (d) indicates the phase-angle bin, with the bin-center angles (color) being 92° (turquoise), 185° (green) and 0° (brown).

The phase-shift error, ε_{ps}, is found for both the SXR and Lyman-α measurements and defined as the standard deviation of the percent difference between the MAVEN/EUVM measurements and the phase-shifted Earth measurements (i.e. the measurements shown in Figures 1b and 1d). All days where data are available between 1 January 2015 and 31 December 2017 are used to calculate ε_{ps}. The data are partitioned according to phase-angle to control for its influence. The three phase-angle bins span $0^o \pm 40^o$, $92^o \pm 40^o$ and $185^o \pm 40^o$. The color bars at the top of Figures 1b and 1d show the phase-angle, where turquoise, green and brown correspond with the bins centered at 92^o, 185^o and 0^o, respectively. For each partitioned dataset, ε_{ps} is found by resampling the data (with replacement) 1000 times using the Bootstrap Method [Efron, 1979]. The resulting values, in percent units, are $\varepsilon_{ps,0}= 1.0 \pm 0.3$ %, $\varepsilon_{ps,92}= 2.1 \pm 0.4$ % and $\varepsilon_{ps,185}= 1.9 \pm 0.1$ % for the Lyman-α band; and $\varepsilon_{ps,0}= 12 \pm 2$ %, $\varepsilon_{ps,92}= 21 \pm 4$ % and $\varepsilon_{ps,185}= 31 \pm 3$ % for the SXR band, where the subscript indicates the phase-angle for each value of ε_{ps}. Since values for ε_{ps} are much larger than σ_{cal}, the reported values are statistically significant.

Since ε_{ps} arises from variability occurring at time-scales shorter than the 27.27 synodic solar rotation period, it is assumed that it is approximately proportional to variability occurring over a solar rotation. We can use this assumption to extend the ε_{ps} values found at the SXR and Lyman-α bands to the full EUV solar spectrum. The solar rotation variability, Δ_{27}, is found by first constructing the following time series of percent variability, *V(t)*,

$$V(t) = \frac{E(t)-E(t+27)}{E(t)} \times 100\%, \qquad (1)$$

where *E(t)* is the irradiance on day *t*. Δ_{27} is defined as the standard deviation of *V(t)*. Δ_{27} is calculated for the solar spectrum at 1 nm binning using spectral irradiance measurements from TIMED/SEE and SDO/EVE. SDO/EVE data from 30 April 2010 through 20 May 2014 are used for the 6 to 30 nm range and TIMED/SEE data from 8 February 2002 through 1 January 2008 are used for the 30 to 190 nm range. The resulting Δ_{27} values are shown in Figure 2a.

By assuming proportionality between Δ_{27} and ε_{ps}, their values at the SXR and Lyman-α bands can be fit to find the functional relationship between the two and, hence, enable the calculation of ε_{ps} from Δ_{27}. Values for Δ_{27} are calculated for the MAVEN/EUVM SXR and Lyman-α bands and fits are found between Δ_{27} and the three phase-angle partitioned ε_{ps} values. This fits are shown in Figure 2b, yielding the following relationships between Δ_{27} and ε_{ps}:

$$\varepsilon_{ps,0} = 0.42 \times \Delta_{27} + 0.06\% \qquad (2.a)$$

$$\varepsilon_{ps,0} = 0.71 \times \Delta_{27} + 0.44\% \qquad (2.b)$$

$$\varepsilon_{ps,0} = 1.11 \times \Delta_{27} - 0.62\% \qquad (2.c)$$

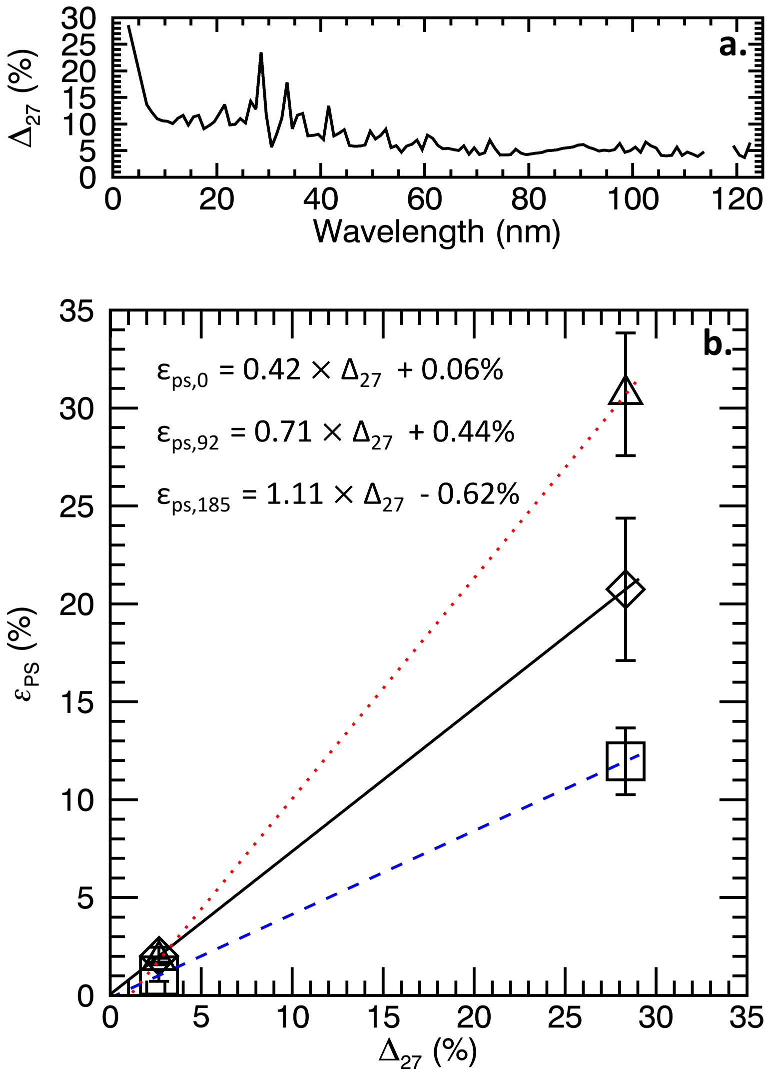

Figure 2. (a) The solar rotation variability (Δ_{27}) at 1 nm sampling derived from EVE and SEE measurements. (b) The linear relationship between the phase-shift error (ε_{ps}) and Δ_{27} derived from the EUVM SXR and Lyman-α bands.

3 Results

Equations (2.a) – (2.c) are used with the results in Figure 2a to estimate ε_{ps} as a function of wavelength for the three phase-angle bins, the values for which are plotted in Figure 3a. This figure shows that ε_{ps} tends to decrease with increasing wavelength. For example, $\varepsilon_{ps,92}$ decreases from a maximum near 20% at the shortest wavelengths to below 3% at 121 nm. Although these values appear small, they should be considered in the context of typical variability as a function of wavelength to understand the impact of extrapolating Earth measured irradiances on a given application. Figure 3 also shows the ratio (in percent units) of ε_{ps} to (b) typical variability occurring over an 11 year solar cycle, σ_{SC}, and (c) typical variability occurring over solar rotation time-scales, σ_{SR}. σ_{SC} is defined as

$$\sigma_{SC} = \frac{\mathrm{StdDev}[E(\mathrm{t})]}{<E(\mathrm{t})>} \times 100\%. \quad (3)$$

σ_{SR} is found by first decomposing the solar variability into solar cycle, E_{SC}, and solar rotation, E_{SR}, variability components where

$$E_{SC}(t) = \langle E(t) \rangle_{55\ day} \quad (4)$$

and

$$E_{SR}(t) = E(t) - E_{SC}(t). \quad (5)$$

With these values defined,

$$\sigma_{SR} = \mathrm{StdDev}\left[\frac{E(t)_{SR}}{E(t)_{SC}}\right] \times 100\%. \quad (6)$$

Over the wavelength range shown, $\varepsilon_{ps,92}$ is approximately one-quarter to one-half of σ_{SR}, and exceeds σ_{SR} below 30 nm, decreasing to ~75% of σ_{SR} near Lyman-α.

Table 1. Error in photoionization frequency (PIF) calculations due phase-shift error for 5 species of aeronomic interest. ε_{PIF} is the error in absolute units. Columns 3-5 report ε_{PIF} relative to the solar cycle mean, solar cycle variability and solar rotation variability, respectively, in percent units.

Value	**$\varepsilon_{ps,92}$ (abs)**	**$\varepsilon_{ps,92}$ (%)**	**$\varepsilon_{ps,92}$ /σ_{SC} (%)**	**$\varepsilon_{ps,92}$ /σ_{SR} (%)**	**ε_{EVE} (%)**	**ε_{EUVM} (%)**	**ε_{LP} (%)**
$E_{0\text{-}103}$	0.321 mW/m^2	7.87	38.2	95.3	1.66	5.27	9.79
PIF_{CO2}	6.15×10^{-08} s^{-1}	5.72	33.0	87.6	1.66	5.1	7.83
PIF_{N2}	3.66×10^{-08} s^{-1}	5.95	33.6	88.7	1.33	5.41	8.13
PIF_{O}	2.46×10^{-08} s^{-1}	5.98	33.1	88.5	1.35	5.17	8.27
PIF_{H2}	5.84×10^{-09} s^{-1}	4.3	29.4	79.7	1.10	4.94	10.6
PIF_{H}	8.1×10^{-09} s^{-1}	7.47	29.4	89.9	3.13	5.39	6.11

It is not clear from Figure 3 how the wavelength dependent error impacts parameters of aeronomic interest. To gain further insight, $\varepsilon_{ps,92}$ (λ) is propagated through calculations of the total ionizing irradiance (using the O_2 ionization threshold potential of 102.8 nm as the long wavelength cutoff) and photoionization frequencies (PIF) for major species in many upper and tenuous planetary atmospheres. Four values are reported for ε_{ps} for each parameter: (1) Absolute units assuming solar-cycle mean irradiance, (2) percent units relative to solar-cycle mean irradiance, and percent units relative to the photoionization variability over (3) solar cycle and (4) solar rotation time scales. Additionally, other sources of error are reported in the rightmost 3 columns of Table 1: ε_{EVE} is the error due to the random uncertainty of the SDO/EVE spectral irradiance measurements; ε_{EUVM} is the error due to the random uncertainty of the MAVEN/EUVM Level 3 spectral irradiance measurements; and ε_{LP} is the random uncertainty of the MAVEN/EUVM Level 3 spectral model driven by the Brace et al., 1988 Langmuir probe derived EUV spectrum. ε_{LP} is found by first creating synthetic photocurrent measurements using the photoemission response curves reported in Brace et al., 1988 and SDO/EVE measured irradiances. A spectral irradiance model calibrated to be driven by this synthetic photocurrent is then developed applying the same methods that were used for the MAVEN/EUVM Level 3 spectral irradiance model described in Thiemann et al., [2017].

It is important to note that ε_{ps} is only the random uncertainty due to the phase-shift error and the total random uncertainty is the quadrature sum of ε_{ps} and the random uncertainty inherent in the irradiance spectra to be phase-shifted. For example, if SDO/EVE measured irradiances are phase-shifted to another planet, then the total random uncertainty is $\sqrt{\varepsilon_{PS} + \varepsilon_{EVE}}$.

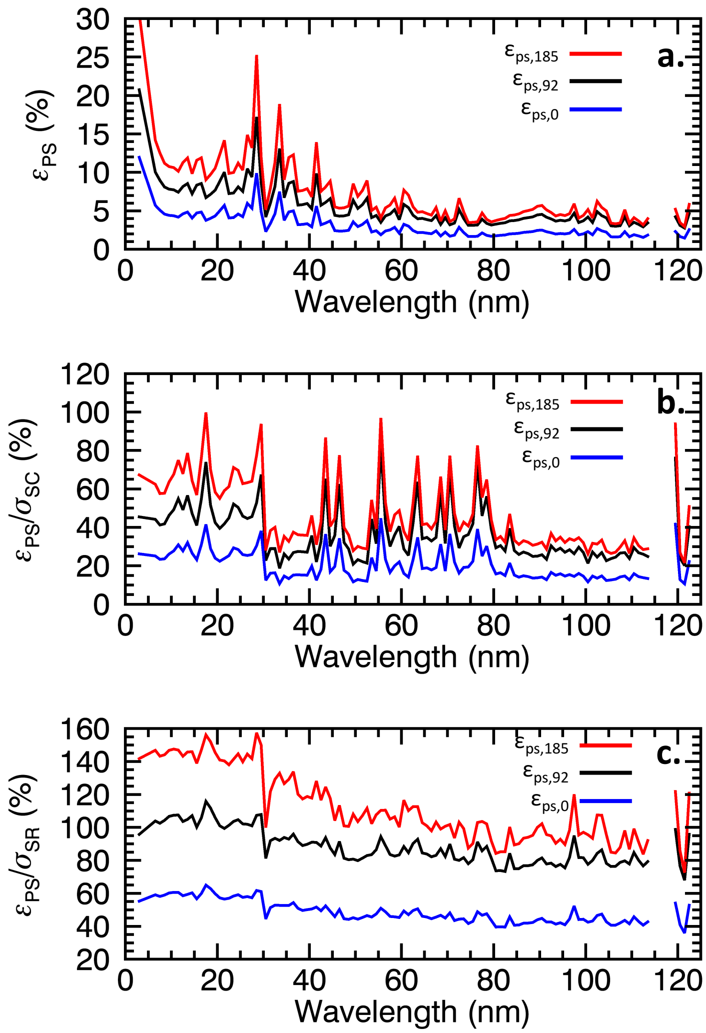

Figure 3. (a) The phase-shift error (ε_{ps}) for extrapolating Earth measured irradiance to other heliographic longitudes in units of percent irradiance. (b) ε_{ps} relative to the variability over long (> ~1 year) timescales. (c) ε_{ps} relative to the variability over short (< ~ 1 month) time-scales.

4 Discussion and Conclusions

The practical import of ε_{ps} depends on the context in which the EUV irradiance estimates are being used as well as the time scale of the analysis. For studies investigating average phenomena over the course of a solar cycle, ε_{ps} may be negligible compared to other sources of error. However, many studies that consider solar EUV irradiance are concerned with understanding whether a causal relation exists between solar EUV irradiance and some other phenomenon. For studies such as these, ε_{ps} may be a major source of uncertainty. From Figure 3 and Table 1, ε_{ps} is 20 to 50% of the variability occurring over an ~11-year solar cycle, which is applicable to studies involving multiple years of data, while ε_{ps} is comparable to the size of the variability occurring over a ~27-day solar rotation. This is particularly relevant for analyses of ground-based observations, which often focus on observations spanning a few weeks.

Considering shorter timescales, the impacts of solar flares are not fully captured by the uncertainties reported in Table 1 because the daily averages from which they are derived suppress the transient enhancements that occur during solar flares. This can be mitigated to some extent if a flare is also visible to Earth via the National Oceanic and Atmospheric Administration (NOAA) Geostationary Operational Environmental Satellites (GOES) X-Ray Sensor, but only in situ irradiance observations can conclusively identify solar flare occurrences [e.g. Thiemann et al., 2015], including Langmuir probe photoemission currents, which have also been demonstrated as capable of observing solar flare occurrences [Johansson et al., 2017; Edberg et al., 2019].

ε_{EUVM} is representative of the random uncertainty of typical spectral irradiance models driven by direct EUV measurements. For example, the state-of-the-art EUV Sensor (EUVS) Model onboard the GOES-R series satellites maintained by NOAA for space weather operations has comparable uncertainties [Thiemann et al., 2019]. As such, when spectral irradiances are estimated by a spectral irradiance model driven with Earth measurements and then phase-shifted to a planetary body of interest, the random uncertainty approximately doubles. Since spectral irradiance models have been used during the majority of the Space Age to predict spectral irradiances at Earth (to compensate for a lack of direct spectral measurements), and this trend is expected to continue with the availability of the NOAA EUVS Model, it generally holds that measuring EUV irradiance in situ, as in the case of MAVEN/EUVM, reduces the random uncertainty by approximately half. From Table 1, it is evident that even the Langmuir probe derived spectral irradiance model has random uncertainties less than $2 \times \varepsilon_{ps,92}$, indicating even relatively crude in-situ irradiance measurements are an improvement upon phase-shifting irradiances from Earth.

The F10.7 solar index is a widely used proxy for solar irradiance; however, it is important to note that F10.7 is only loosely correlated with solar EUV irradiance when used directly. For example, Chamberlin et al. [2007] showed that EUV irradiance model random uncertainty between 30 and 90 nm increases by a factor of ~15 when the F10.7 index is used directly versus EUV measurements as the model input. As such, ε_{ps} is only a secondary contribution to the random uncertainty associated with the F10.7 index when used directly as a proxy for EUV irradiance. Note, this only pertains to models that use F10.7 directly such as the EUV for Aeronomic Calculations (EUVAC; Richards et al. 1994) model. More sophisticated models such as that by Hinteregger et al., [1981] decompose the F10.7 index into short and long term components, and these models have random uncertainties that are approximately twice that of models driven with EUV measurements [Cesseteur et al., 2011].

Solar Lyman-α irradiance is an important constraint for analyses of planetary and interplanetary hydrogen observations [Anderson and Hord, 1971; Quemerais et al., 2003; Gladstone et al., 2004; Chaufray et al., 2012]. Hydrogen is observed by measuring resonantly scattered Lyman-α photons of solar origin. In many applications, hydrogen emissions are optically thick (due to the large abundance of hydrogen in the solar system), resulting in a nonlinear relation between the retrieved hydrogen densities and the assumed incident solar Lyman-α irradiance, and an increased sensitivity to the absolute irradiance calibration. Chaufray et al., [2008] showed that in the case of retrieving hydrogen densities from Lyman-α emissions at Mars, a 10% error in the assumed solar Lyman-α irradiance changed the retrieved hydrogen densities by a factors 0.4 to 3.25 for the 7 orbits analyzed. As such, the impact of ε_{ps} on H density retrievals may be much larger than the ~2% magnitude of ε_{ps} at 121.6 nm, and ε_{ps} likely needs to be propagated through the relevant retrieval algorithms on a case by case basis in order to quantify its relative impact on hydrogen observations.

ε_{ps} increases for larger phase-angles as is to be expected. For phase-angles near 180°, ε_{ps} varies by 100-140% of the typical 27-day variability below 100 nm. This decreases to 50% for phase-angles less than 40°, and obviously approaches 0% as the phase-angle approaches 0°. This implies that correlations between a quantity of interest and solar EUV irradiance may be significantly masked by phase-shifting error when the phase-shift angle exceeds ~135°.

Acknowledgments

EMBT thanks Dr. Leonid Didkovsky of the University of Southern California for his assistance in interpreting the SDO/ESP data.

Version 12, Revision 2 MAVEN/EUVM data were used and are publicly available through the Atmospheres node on the NASA Planetary Data System. Version 12 TIMED/SEE data were used and are available on the web at http://lasp.colorado.edu/home/see/data/. Version 6 SDO/EVE data were used and are available on the web at http://lasp.colorado.edu/eve/data_access/index.html.

Atmospheric cross-sections for calculating the photoionization frequencies were downloaded from the Photo Ionization/Dissociation Rates (PHIDRATES) database publicly available on the web at https://phidrates.space.swri.edu/ and documented in Huebner and Mukherjee [2015].

This work was funded by NASA Living with a Star Grant NNX16AE86G, and the NASA MAVEN project.

References

Anderson Jr, D. E., & Hord, C. W. (1971). Mariner 6 and 7 ultraviolet spectrometer experiment: Analysis of hydrogen Lyman-alpha data. *Journal of Geophysical Research*, *76*(28), 6666-6673.

Arge, C. N., Henney, C. J., Koller, J., Compeau, C. R., Young, S., MacKenzie, D., ... & Harvey, J. W. (2010, March). Air force data assimilative photospheric flux transport (ADAPT) model. In *AIP Conference Proceedings* (Vol. 1216, No. 1, pp. 343-346). American Institute of Physics

Brace, L. H., Hoegy, W. R., & Theis, R. F. (1988). Solar EUV measurements at Venus based on photoelectron emission from the Pioneer Venus Langmuir probe. *Journal of Geophysical Research: Space Physics*, *93*(A7), 7282-7296.

Cessateur, G., de Wit, T. D., Kretzschmar, M., Lilensten, J., Hochedez, J. F., & Snow, M. (2011). Monitoring the solar UV irradiance spectrum from the observation of a few passbands. *Astronomy & Astrophysics*, *528*, A68

Chamberlin, P. C., Woods, T. N., & Eparvier, F. G. (2007). Flare irradiance spectral model (FISM): Daily component algorithms and results. *Space Weather*, *5*(7).

Chamberlin, P. C., Woods, T. N., Didkovsky, L., Eparvier, F. G., Jones, A. R., Machol, J. L., ... & Woodraska, D. L. (2018). Solar ultraviolet irradiance observations of the solar flares during the intense September 2017 storm period. *Space Weather*, *16*(10), 1470-1487.

Chaufray, J. Y., Bertaux, J. L., Quémerais, E., Villard, E., & Leblanc, F. (2012). Hydrogen density in the dayside venusian exosphere derived from Lyman-α observations by SPICAV on Venus Express. *Icarus*, *217*(2), 767-778.

Chaufray, J. Y., Bertaux, J. L., Leblanc, F., & Quémerais, E. (2008). Observation of the hydrogen corona with SPICAM on Mars Express. *Icarus*, *195*(2), 598-613.

Didkovsky, L., Judge, D., Wieman, S., Woods, T., & Jones, A. (2009). EUV spectrophotometer (ESP) in extreme ultraviolet variability experiment (EVE): algorithms and calibrations. In *The Solar Dynamics Observatory* (pp. 179-205). Springer, New York, NY.

Edberg, N. J., Johansson, F. L., Eriksson, A. I., Andrews, D. J., Hajra, R., Henri, P., ... & Thiemann, E. (2019). Solar flares observed by Rosetta at comet 67P/Churyumov-Gerasimenko. *Astronomy & Astrophysics*, *630*, A49.

Efron, B. (1979). Bootstrap methods: another look at the jackknife annals of statistics 7: 1–26.

Eparvier, F. G., Chamberlin, P. C., Woods, T. N., & Thiemann, E. M. B. (2015). The solar extreme ultraviolet monitor for MAVEN. *Space Science Reviews*, *195*(1-4), 293-301.

Gladstone, G. R., Pryor, W. R., Tobiska, W. K., Stewart, A. I. F., Simmons, K. E., & Ajello, J. M. (2004). Constraints on Jupiter's hydrogen corona from Galileo UVS observations. *Planetary and Space Science*, *52*(5-6), 415-421.

Hinteregger, Hans E., Katsura Fukui, and Bruce R. Gilson. "Observational, reference and model data on solar EUV, from measurements on AE-E." *Geophysical Research Letters* 8.11 (1981): 1147-1150.

Huebner, W. F., & Mukherjee, J. (2015). Photoionization and photodissociation rates in solar and blackbody radiation fields. *Planetary and Space Science*, *106*, 11-45.

Jakosky, B. M., Lin, R. P., Grebowsky, J. M., Luhmann, J. G., Mitchell, D. F., Beutelschies, G., ... & Baker, D. (2015). The Mars atmosphere and volatile evolution (MAVEN) mission. *Space Science Reviews*, *195*(1-4), 3-48.

Johansson, F. L., Odelstad, E., Paulsson, J. J. P., Harang, S. S., Eriksson, A. I., Mannel, T., ... & Thiemann, E. (2017). Rosetta photoelectron emission and solar ultraviolet flux at comet 67P. *Monthly Notices of the Royal Astronomical Society*, *469*(Suppl_2), S626-S635.

Killen, R. M., Potter, A. E., Reiff, P., Sarantos, M., Jackson, B. V., Hick, P., & Giles, B. (2001). Evidence for space weather at Mercury. *Journal of Geophysical Research: Planets*, *106*(E9), 20509-20525.

McClintock, W. E., Rottman, G. J., & Woods, T. N. (2005). Solar–Stellar Irradiance Comparison Experiment II (SOLSTICE II): Instrument concept and design. *Solar Physics*, *230*(1-2), 225-258.

Moore, L., Galand, M., Mueller-Wodarg, I., & Mendillo, M. (2009). Response of Saturn's ionosphere to solar radiation: Testing parameterizations for thermal electron heating and secondary ionization processes. *Planetary and Space Science*, *57*(14-15), 1699-1705.

Parkinson, C. D., McConnell, J. C., Sandel, B. R., Yelle, R. V., & Broadfoot, A. L. (1990). He 584 Å dayglow at Neptune. *Geophysical research letters*, *17*(10), 1709-1712.

Peter, K., Pätzold, M., Molina-Cuberos, G., Witasse, O., González-Galindo, F., Withers, P., ... & Tyler, G. L. (2014). The dayside ionospheres of Mars and Venus: Comparing a one-dimensional photochemical model with MaRS (Mars Express) and VeRa (Venus Express) observations. *Icarus*, *233*, 66-82.

Ramstad, R., Barabash, S., Futaana, Y., Nilsson, H., Wang, X. D., & Holmström, M. (2015). The Martian atmospheric ion escape rate dependence on solar wind and solar EUV conditions: 1. Seven years of Mars Express observations. *Journal of Geophysical Research: Planets*, *120*(7), 1298-1309.

Richards, P. G., Fennelly, J. A., & Torr, D. G. (1994). EUVAC: A solar EUV flux model for aeronomic calculations. *Journal of Geophysical Research: Space Physics*, *99*(A5), 8981-8992.

Quémerais, E., Bertaux, J. L., Lallement, R., Sandel, B. R., & Izmodenov, V. (2003). Voyager 1/UVS Lyman α glow data from 1993 to 2003: Hydrogen distribution in the upwind outer heliosphere. *Journal of Geophysical Research: Space Physics*, *108*(A10).

Thiemann, E. M. B., Eparvier, F. G., Andersson, L. A., Fowler, C. M., Peterson, W. K., Mahaffy, P. R., ... & Deighan, J. I. (2015). Neutral density response to solar flares at Mars. *Geophysical Research Letters*, *42*(21), 8986-8992.

Thiemann, E. M. (2016). *Multi-spectral sensor driven solar EUV irradiance models with improved spectro-temporal resolution for space weather applications at Earth and Mars* (Doctoral dissertation, University of Colorado at Boulder)

Thiemann, E. M., Chamberlin, P. C., Eparvier, F. G., Templeman, B., Woods, T. N., Bougher, S. W., & Jakosky, B. M. (2017). The MAVEN EUVM model of solar spectral irradiance variability at Mars: Algorithms and results. *Journal of Geophysical Research: Space Physics*, *122*(3), 2748-2767.

Thiemann, E. M. B., Andersson, L., Lillis, R., Withers, P., Xu, S., Elrod, M., ... & Eparvier, F. G. (2018a). The Mars topside ionosphere response to the X8. 2 solar flare of 10 September 2017. *Geophysical Research Letters*, *45*(16), 8005-8013.

Thiemann, E. M. B., Chamberlin, P. C., Eparvier, F. G., & Epp, L. (2018b). Center-to-limb variability of hot coronal EUV emissions during solar flares. *Solar Physics*, *293*(2), 19.

Thiemann, E. M., Eparvier, F. G., Woodraska, D., Chamberlin, P. C., Machol, J., Eden, T., ... & Viereck, R. (2019). The GOES-R EUVS model for EUV irradiance variability. *Journal of Space Weather and Space Climate*, *9*, A43.

Trafton, L. M., & Stern, S. A. (1996). Rotationally resolved spectral studies of Pluto from 2500 to 4800 angstroms obtained with HST. *The Astronomical Journal*, *112*, 1212.

Tsuchiya, F., Misawa, H., Imai, K., & Morioka, A. (2011). Short-term changes in Jupiter's synchrotron radiation at 325 MHz: Enhanced radial diffusion in Jupiter's radiation belt driven by solar UV/EUV heating. *Journal of Geophysical Research: Space Physics*, *116*(A9).

Woods, T. N., Eparvier, F. G., Fontenla, J., Harder, J., Kopp, G., McClintock, W. E., ... & Snow, M. (2004). Solar irradiance variability during the October 2003 solar storm period. *Geophysical research letters*, *31*(10).

Woods, T. N., Eparvier, F. G., Bailey, S. M., Chamberlin, P. C., Lean, J., Rottman, G. J., ... & Woodraska, D. L. (2005). Solar EUV Experiment (SEE): Mission overview and first results. *Journal of Geophysical Research: Space Physics*, *110*(A1).

Woods, T. N., Eparvier, F. G., Hock, R., Jones, A. R., Woodraska, D., Judge, D., ... & McMullin, D. (2010). Extreme Ultraviolet Variability Experiment (EVE) on the Solar Dynamics Observatory (SDO): Overview of science objectives, instrument design, data products, and model developments. In *The solar dynamics observatory* (pp. 115-143). Springer, New York, NY.

Woods, T. N., Eparvier, F. G., Harder, J., & Snow, M. (2018). Decoupling solar variability and instrument trends using the multiple same-irradiance-level (MuSIL) analysis technique. *Solar physics*, *293*(5), 76.